Time Allocation and Optimization in UAV-enabled Wireless Powered Communication Networks

Hua Yan, *Graduate Student Member, IEEE*, Yunfei Chen and Shuang-Hua Yang, *Senior Member, IEEE*

***Abstract*—Unmanned aerial vehicles (UAVs) have attracted great research attention due to their flexibility. In this paper, the use of UAVs in wireless sensor networks as an energy transmitter and a data collector is investigated. The UAV is first charged from a charging station, such as a base station (BS), before it flies to the sensors for data collection. Upon arrival, the UAV first charges the sensors via wireless power transfer (WPT) in the downlink, followed by data transmission from the sensors in the uplink. After that, the UAV flies back to the BS to offload data to the BS. We aim to maximize the amount of data offloaded to the BS by allocating optimal time slots to different tasks in this process, given a fixed total time. The maximization is solved in two steps as two convex optimization problems. In the first step, the time allocation between WPT to sensors and data collection from sensors is optimized. In the second step, the time allocation of BS charging, the total time in the first step, and BS data offloading is optimized. Unlike the previous works, our study takes into account the charging process from the BS to the UAV, the propulsion consumption at the UAV and the data offloading process to the BS. Both distance-dependent path loss and small-scale fading are considered. Numerical results show that the optimal time allocation can maximize the amount of data at the BS without wasting any time and energy.**

***Index Terms*—Data collection, sensor, unmanned aerial vehicle (UAV), wireless power transfer (WPT).**

I. Introduction

A. Background and Challenges

RECENTLY, unmanned aerial vehicles (UAVs) have been presenting a promising technology in 5G, Internet of Things (IoTs) and the six-generation (6G) communication networks [1], [2]. In particular, there has been a growing interest in studying UAV-enabled wireless powered communication networks (WPCNs) [3] – [4], where the UAV was dispatched to collect data from remote sensors, charge remote sensors or both [3] – [8]. For example, the authors in [3] combined the wireless power transfer (WPT) and wireless information transfer (WIT) in a WPCN, where a UAV with a constant power supply coordinated the WPT/WIT to/from a set of ground users. The uplink (UL) sum-rate was maximized by jointly optimizing time allocation and the UAV position. In [4], the outage probability of the UAV-enabled WPCN was analysed by identifying the optimum time ratio of the WPT and the WIT under the assumption of the Rician fading channel. The authors in [5] employed UAVs to collect data from the sensors as well as recharge the sensors. In [6], a UAV was used as a flying base station to serve battery-limited sensors. Both data collection and sensor charging have been studied. In [7], a novel energy-efficient data collection and WPT system using a multiple-input multiple-output (MIMO) full-duplex (FD) UAV was proposed, where simultaneous wireless information and power transfer was explored. In [8], the outage and coverage performance of the UAV-aided WPT and data collection have been studied, where the Rician fading and path loss caused by UAV's elevation angle were considered. In practical applications, one challenge is to schedule the full process of a UAV mission when considering its own energy supply and propulsion in a given time. That is, the UAV is first charged with a certain amount of energy by a charging station and then dispatched to charge the remote sensors, and then collect data from sensors and bring it back to the charging station. There may exist an optimal time allocation at different phases of this full process.

This work was supported in part by the National Key Research and Development Program of China under Grant 2019YFC0810705; in part by the National Natural Science Foundation of China under Grant 61873119 and Grant 92067109; and in part by the Science and Technology Innovation Commission of Shenzhen under Grant KQJSCX20180322151418232. *(Corresponding author: Shuang-Hua Yang)*

H. Yan and Y. Chen are with the School of Engineering, University of Warwick, Coventry, U.K. CV4 7AL (e-mail: Hua.Yan@warwick.ac.uk and Yunfei.Chen@warwick.ac.uk).

S. Yang is with the Department of Computer Science and Engineering, Southern University of Science and Technology, Shenzhen 518055, China, and also with PCL Research Center of Networks and Communications, Peng Cheng Laboratory, Shenzhen 518055, China (e-mail: yangsh@sustech.edu.cn).

B. Related work

In view of the fact that UAVs can be flexibly deployed on-demand when required, UAV-aided data collection has attained significant research attention. The authors in [9] proposed a novel UAV-aided sensor network, where a UAV was employed as a mobile data collector for data collection and also as an anchor node to help terrestrial base station (BS) with sensor positioning. Similarly, a UAV-aided data collection scheme for wireless sensor networks (WSNs) was studied in [10], where both single UAV and multiple UAVs were considered. In [11], a UAV-enabled WSN was studied, where a flying UAV was dispatched to collect data from multiple sensors, and the minimum average data rate was maximized via optimizing the UAV communication scheduling and 3D trajectory. In [12], the shortest path for UAV-aided data collection was derived to achieve a high delivery rate and a low energy usage. Reference [13] studied UAV-aided data collection from time-constrained sensors via jointly optimizing the trajectory of the UAV and the radio resource allocation. In [14], UAV operations and traffic data collection have been reviewed for driving behaviour analysis. In [15], energy-efficient data collection was studied, where sensor wake-up schedule and UAV trajectory were jointly optimized to minimize the maximum energy consumption for all sensors. Furthermore, reference [16] extended the work in [15] to multiple UAVs, in which the mission completion time among all UAVs was minimized. In [17], a UAV was dispatched to collect data from a set of sensors distributed on a straight line. The total flight time of the UAV was minimized via jointly optimizing sensor transmit power and the UAV speed.

The authors in [18] proposed four UAV-aided data collection algorithms considering the dynamic network topology where sensors were mobile with constant velocities. In [19], a UAV trajectory planning model for data collection was proposed taking into account the message expiration. Also, in [20], age of information was considered as a performance metric to measure the data freshness in UAV-aided IoT networks. In [21], a UAV-aided data collection design was proposed, where the UAV's trajectory, velocity, altitude and data link were all considered to minimize the mission time. In [22], a UAV acting as a mobile sink was dispatched to collect data from the cluster node of a WSN, and a direct future prediction model was proposed for UAV's trajectory plan. In [23], a rotary-wing UAV with limited onboard energy was employed to collect data from sensors. The maximum energy consumption among all sensors was minimized by jointly optimizing the communication schedule, the transmit power and the UAV trajectory.

As sensors deployed in IoTs are energy-limited nodes and they need to be charged until the energy exceeds the circuit activation threshold to start transmitting data [8], works on UAV-enabled WPCNs [3] – [8] began to study the performance of combining WPT and data collection. Similarly, considering the UAV consumes energy in different manoeuvres, some recent works have started to take UAV propulsion energy into account [24] – [25]. In [24], a rotary-wing UAV equipped with a hybrid access point was employed to serve energy-limited sensors, where sum throughput problem, total time minimization problem and total energy minimization (TEM) problem were optimized. For the TEM problem, UAV's propulsion energy was considered. Similarly, in [25], a rotary-wing UAV considering propulsion energy was considered to serve multiple ground users, where the ground users first harvested radio frequency energy from the UAV, and then transmitted information to the UAV. The energy-time trade-off was solved by jointly optimizing the user scheduling, UAV trajectory and mission completion time.

C. Motivation and Contributions

All these works have provided very valuable insights on the use of UAV-enabled WPT and data collection. However, in these works, there are three important issues that have been more or less ignored. Firstly, the power consumption of the UAV has not been considered in most of these applications [3] – [17]. This affects the operational efficiency of the UAV. Secondly, UAV is an energy-limited node that does not generate energy itself. All these works [3] – [25] have ignored the energy charging process from a charging station[1], such as a BS, to the UAV, either with wired power supply or wirelessly. In [27], UAV energy harvesting from solar energy or wind energy has been studied. However, the amount of energy harvested is random and thus, it may not be enough as the main energy source of the UAV, but as a supplement, it could be a good choice. Also, data collection has not been considered in this work. Thirdly, the purpose of collecting data from the sensors is to offload them to the BS, i.e., the mobile edge computing (MEC) server [28], [29], for computing and decision-making [8]. Thus, data offloading at the BS is an important process that has been ignored in these works. To the best of the authors' knowledge, UAV-aided WPT and data collection considering all these three important issues has not been studied yet and thus, it represents contribution.

Motivated by the above observations, this paper studies the use of the UAV in a WPCN serving as both a data collector and a wireless energy transmitter. In the study, the energy consumption at the UAV, the energy transfer from the BS to the UAV, and the data offloading from the UAV to the BS will all be considered along with other processes in the UAV-enabled WPCN. In detail, four phases are needed to be considered. First, since the UAV does not generate energy itself, it needs to be firstly charged by a charge station, i.e., a BS, and then flies to the sensors at the cost of propulsion consumption. Second, the UAV, upon arrival, first charges all the sensors distributed in a given area in the downlink (DL) as all sensors are assumed to be in a low power state with solar energy acquisition capability and can only be used for sensing, followed by data transmission from the sensors to the UAV in the UL in a time-division-multiple-access (TDMA) manner. This is the third phase. Note that, for one sensor, simultaneously WPT and data collection could save time. However, in practical applications, there are usually multiple sensors. To avoid the inter-user interference caused by data transmission among different sensors, TDMA is employed [8], [30]. After data collection, the UAV flies back to the BS with propulsion energy consumption again, and offloads the collected data to the BS for further processing in the fourth phase. In the study, both distance-dependent path loss and small-scale fading are considered to maximize the data volume and transmission efficiency, defined as the ratio of the amount of data offloaded to the BS to the amount of data collected from the sensors, given a fixed total time. The closed-form expression for the optimal time allocation between different phases will be derived. Simulation results will be presented to give useful guidance for system designs. The main contributions of this work can be summarized as follows:

- The UAV-enabled sensor network is studied by considering energy transfer from the BS to the UAV, the UAV power consumption and the data offloading from the UAV to the BS.
- The closed-form expressions of the optimal time allocation are derived analytically.
- Two TDMA mechanisms, i.e., TDMA with equal transmission times for all sensors and TDMA with optimal transmission times for all sensors are studied.
- The effects of different system parameters on the transmission efficiency and the optimal time allocation are examined to provide useful guidance for system designs.

The rest of the paper is organized as follows. In Section II, the system model is explained. Section III derives the optimal time allocation. Section IV further discusses and analyses the time allocation problem. Section V presents numerical results. Finally, the work is concluded in Section VI.

II. System Model

Consider a UAV-enabled WPCN. As depicted in Fig. 1, the system consists of one BS, one UAV and K sensors distributed in a given area and denoted by S_k with $1 \leq k \leq K$. All the sensors are assumed to be located on a two-dimensional (2D)

[1]Note that UAV can be recharged wirelessly by a wireless charger without landing, and the output power of the wireless charger can reach 12 KW [26].

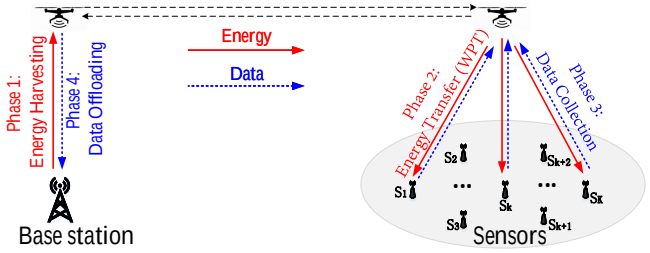

Fig. 1. Illustration of system model.

surface. The position of the BS is denoted as $(0, 0, H_{bs})$ with a height of H_{bs}. The location of the k^{th} sensor is denoted as (x_k, y_k, H_{sr}) with a common antenna height of H_{sr}. The UAV is assumed to fly at a fixed height of H above the ground [23] – [25], and hence its location can be denoted as (x, y, H). The UAV-aided data collection process works as follows. First, a rotary-wing UAV is charged by a BS wirelessly in its close proximity [26], [31] – [32]. After being charged for a period of time, the UAV flies to the destination area where all sensors are located. Then, the UAV charges all sensors via WPT in the DL for a certain period of time, followed by the orthogonal data transmission from the sensors to the UAV in the UL in a TDMA manner. Finally, the UAV flies back to the BS and offloads data to the BS wirelessly. The main reason for the use of UAV, instead of performing WPT and data collection directly between the BS and the sensors [30] – [33], is to reduce the transmission range and therefore to improve the efficiency of the BS and sensor operations, as the path loss will be greatly reduced by performing transmission and reception in a close proximity [31] – [32].

In this work, we assume wireless charging by the BS to the UAV [31] – [32], [34]. This is the case when there is no dedicated landing dock at the BS for wired charging, as in conventional BSs. This is also the case when it is not convenient or safe for the UAV to land due to the complicated environment surrounding the BS. In the case when wired charging is available at the BS, the following results are still valid by ignoring the first phase of the BS charging or by assuming a very high conversion efficiency. Besides, one wireless charging station can charge multiple UAVs at the same time, which is an advantage over wired charging on the ground [26].

As shown in Fig. 1, the communication link between the BS and the UAV as well as that between the UAV and sensors on the ground are assumed to be dominated by line-of-sight (LoS). This is another benefit of using UAVs. In this case, the propagation model encompasses both the distance-dependent path loss and small-scale fading. It may be noted that there have been path loss models for UAVs [35] – [36]. However, fading was ignored in these works. In our paper, we assume Rician fading [4], [8], [37]. We consider WPT from the BS to the UAV in Phase 1 and from the UAV to the sensors in Phase 2. Consequently, data collection from ground sensors to the UAV is considered in Phase 3 after charging sensors, and data offloading from the UAV to the BS is considered in Phase 4. Note that there is also a round-trip flight, i.e., the UAV flies to the sensors after harvesting energy from the BS in Phase 1, and flies back to the BS after collecting data from the sensors in Phase 3. The goal is to derive the optimal time allocation for these four phases given a fixed flight distance and a fixed total time. The round-trip process is not included in the time allocation, as the flight time is determined by the flight distance and UAV speed and both are fixed.

A. Phase 1 – Energy harvesting

In Phase 1, the BS charges the UAV, as shown in Fig. 1. The received power in dB at the UAV due to path loss can be expressed as [31], [32]

$$P_{uav-r} = P_{bs-t} + G_{bs} + G_{uav} - PL_{bs-uav}, \tag{1}$$

where P_{bs-t} denotes the transmit power at the BS, G_{bs} and G_{uav} are the antenna gains of the BS and the UAV in dBi, respectively, $PL_{bs-uav} = 20\lg\{f\} + 20\lg\{d_{bs-uav}\} - 147.55$ dB is the free-space path loss between the BS and the UAV, f denotes the operating frequency, and $d_{bs-uav} = H - H_{bs}$ with $d_{bs-uav} \geq 1$ is the distance between the BS and the UAV for wireless charging in far-field. Let $g_{b,u} \sim \mathcal{CN}(0, \sigma_{b,u}^2)$ denote the complex channel coefficient from the BS to the UAV, where $\sigma_{b,u}^2$ is the average fading power. Thus, the far-field wireless energy harvested by the UAV during Phase 1 can be expressed as

$$E_{uav-h} = \eta 10^{\frac{P_{uav-r}}{10}} |g_{b,u}|^2 T_{phase1}, \tag{2}$$

where $0 < \eta < 1$ is the energy conversion efficiency [38], i.e., radio frequency to direct current (RF-to-DC), at the UAV, and T_{phase1} is the operating time in Phase 1 or the charging time. For time sensitive tasks, such as emergency and rescue, T_{phase1} is usually less than the time to fully charge the UAV. Thus, in a given time, reasonable time allocation may improve the efficiency of UAV missions.

It is worth noting that there are different technologies for UAV wireless charging, such as inductive coupling, magnetic resonance coupling, capacitive coupling, RF power beamforming and laser beaming [39] – [44]. For wired charging, η is close to 1, $g_{b,u} = 1$ and $PL_{bs-uav} = G_{bs} = G_{uav} \approx 0$ dB. For inductive coupling [42], $g_{b,u} = 1$, $PL_{bs-uav} = G_{bs} = G_{uav} \approx 0$ dB, the distance d_{bs-uav} in PL_{bs-uav} can be 3 cm [43], and η can be any value between 0 and 1 depending on P_{uav-r}. For laser beaming [44], $g_{b,u} = 1$, $G_{bs} = G_{uav} \approx 0$ dB, $PL_{bs-uav} = 10\frac{C_\epsilon}{\kappa_v}(\frac{\lambda}{C_\chi})^{-\rho_{sd}} d_{bs-uav} \lg e$ and η can be 0.54 [45], C_ϵ and C_χ are two constants, κ_v is the visibility, λ is the wavelength, ρ_{sd} is the size distribution of the scattering particles and depends on κ_v, and e is the Euler number. Thus, E_{uav-h} in (2) is general and applicable to different transmission powers and distances from the charger. Fig. 2 shows the energy harvested at the UAV via laser charging versus different flight heights under three scenarios [45]. In the figure, $P_{bs-t} = 30$ dBW, $T_{phase1} = 10$ minutes, $\eta = 0.54$, and other parameters follow [45, Table III]. One can see that the energy harvested at the UAV decreases with the UAV flight height. This is due to the fact that PL_{bs-uav} increases with the distance between the BS and the UAV. Besides, the harvested energy is also influenced by weather. When the UAV flight height is fixed at 1 km, one sees that the energy harvested at the UAV in clear air is the largest, followed by in a haze, and in fog. This is because the laser with high frequency is easily obscured by fog. From the global drone regulations database (GDRDB), most countries, such as European countries, USA and China, have a maximum altitude of 120 meters, and Canada

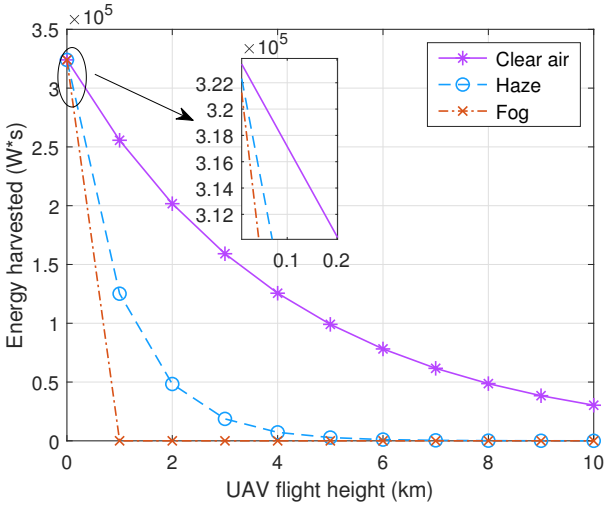

Fig. 2. Energy harvested via laser vs UAV flight heights.

of 90 meters for UAVs [46], and there is no minimum altitude as long as it is reasonable. In China, the flight height of the UAV for assisting agricultural spraying shall not exceed 15 meters [46]. Thus, Fig. 2 shows that at least wireless charging of UAV via laser is promising under the regulations.

B. Phase 2 – WPT

Upon arrival, in Phase 2, the UAV hovers at a height of H above the sensors and broadcasts wireless energy to all sensors on the ground to charge them in the DL. Let P_{uav-t} denote the transmit power at the UAV and $h_{u,k} \sim \mathcal{CN}(0, \sigma_{u,k}^2)$ denote the complex channel coefficient from the UAV to the k^{th} sensor, where $\sigma_{u,k}^2$ is the average fading power. Thus, the received power at the k^{th} sensor in the DL due to path loss can be expressed as

$$P_{k-r} = P_{uav-t} + G_{uav} + G_k - PL_{uav-k}, \tag{3}$$

where $PL_{uav-k} = 20\lg\{f\} + 20\lg\{d_{uav-k}\} - 147.55$ dB is the free-space path loss between the UAV and the k^{th} sensor, $d_{uav-k} = \sqrt{(x-x_k)^2 + (y-y_k)^2 + (H-H_{sr})^2}$ with $d_{uav-k} \geq 1$ is the distance between the UAV and the k^{th} sensor, G_k is the antenna gain of the k^{th} sensor and all other symbols are denoted as before. For convenience, it is assumed that $G_1 = \cdots = G_K = G_{sr}$ in this paper so that all sensors have the same antenna gains. As a result, the amount of energy harvested by the k^{th} sensor is

$$E_k = \eta_k 10^{\frac{P_{k-r}}{10}} |h_{u,k}|^2 T_{phase2}, \tag{4}$$

where T_{phase2} is the charging time for energy replenishing in Phase 2, $0 < \eta_k < 1, k = 1, \ldots, K$, is the energy conversion efficiency at the k^{th} sensor. In most previous works [3] – [4], [24] – [25], it has been assumed that the conversion efficiency is a constant that is linear and independent of the input power whether the input power is large or small. However, it has been revealed that the conversion efficiency actually depends on the input power [38], which means the output harvested power is non-linear. One has the relationship between the input power P_{in} and the output power $f(P_{in})$ of the energy harvester as [38]

$$f(P_{in}) = \frac{a_0 P_{in} + b_0}{P_{in} + c_0} - \frac{b_0}{c_0}, \tag{5}$$

where a_0, b_0 and c_0 are constants obtained by standard curve-fitting. In this case, the conversion efficiency at the k^{th} sensor can be expressed as

$$\eta_k = \frac{f(P_{k-r})}{P_{k-r}}, \quad k = 1, \ldots, K, \tag{6}$$

which changes with the input power, i.e., P_{k-r}, at the k^{th} sensor. Thus, for WPT in Phase 2, we assume an energy conversion efficiency that varies with input power at different sensors. Note that the energy conversion efficiency η in Phase 1 is also non-linear actually, and it is determined by PL_{bs-uav} in (1).

C. Phase 3 – Data collection

After charging the sensors, the UAV will collect data from the sensors using TDMA in the corresponding UL in Phase 3 with a total transmission time of T_{phase3}. It is assumed that all the energy harvested at each sensor will be used for its UL information transmission [30] and that the amount of time allocated for each sensor in the UL is denoted by t_k. Since the total time for Phase 3 is T_{phase3}, we have

$$\sum_{k=1}^{K} t_k \leq T_{phase3}, \ k = 1, \ldots, K. \tag{7}$$

Consequently, the transmission power of the k^{th} sensor, denoted by P_{k-t}, is proportional to E_k in (4). One has

$$P_{k-t} = \frac{E_k}{t_k} = \frac{\eta_k 10^{\frac{P_{k-r}}{10}} |h_{u,k}|^2 T_{phase2}}{t_k}. \tag{8}$$

The received power at the UAV from the k^{th} sensor in the UL due to path loss can be expressed as

$$P_{uav-r_k} = 10\lg\{P_{k-t}\} + G_k + G_{uav} - PL_{uav-k}. \tag{9}$$

We denote $g_{k,u} \sim \mathcal{CN}(0, \sigma_{k,u}^2)$ as the complex channel coefficient from the k^{th} sensor to the UAV. The overall received signal at the UAV in the UL is given by

$$y_{k,u} = \sqrt{10^{\frac{P_{uav-r_k}}{10}}} g_{k,u} s_{k,u} + n_{k,u}, k = 1, \ldots, K, \tag{10}$$

where $s_{k,u}$ is the signal transmitted by the k^{th} sensor with $E\left\{|s_{k,u}|^2\right\} = 1$, and $n_{k,u} \sim \mathcal{CN}(0, \sigma_{k,u}^2)$ is the noise at the UAV during t_k with mean zero and variance $\sigma_{k,u}^2$. From (4) – (10), the sum-data received by UAV from K sensors after Phase 3 can be formulated as

$$D_{K,u} = \sum_{k=1}^{K} t_k \log_2 \left(1 + \frac{10^{\frac{P_{uav-r_k}}{10}} |g_{k,u}|^2}{\sigma_{k,u}^2}\right). \tag{11a}$$

$$\text{s.t.:} \sum_{k=1}^{K} t_k \leq T_{phase3}, \ k = 1, \ldots, K, \tag{11b}$$

D. Phase 4 – Data offloading

In Phase 4, the UAV hovers above the BS for data offloading. The received power at the BS from the UAV due to path loss can be expressed as

$$P_{bs-r} = P_{uav-t} + G_{uav} + G_{bs} - PL_{bs-uav}, \tag{12}$$

where P_{uav-t} is the transmission power of the UAV during data-offloading as that in (3). During Phase 4, let $h_{u,b} \sim \mathcal{CN}(0, \sigma_{u,b}^2)$ denote the complex channel coefficient from the UAV to BS, the overall received signal at the BS from the UAV considering both path loss and fading is

$$y_{u,b} = \sqrt{10^{\frac{P_{bs-r}}{10}}} h_{u,b} s_{u,b} + n_{u,b}, \tag{13}$$

where $s_{u,b}$ is the transmitted signal of the UAV with $E\left\{|s_{u,b}|^2\right\} = 1$, and $n_{u,b} \sim \mathcal{CN}(0, \sigma_{u,b}^2)$ denotes the noise at the BS. Then, the amount of data that can be offloaded at the BS in Phase 4 can be expressed as

$$D_{u,b} = T_{phase4} \log_2 \left(1 + \frac{10^{\frac{P_{bs-r}}{10}} |h_{u,b}|^2}{\sigma_{u,b}^2}\right). \tag{14}$$

E. UAV Propulsion Consumption for round-trip flight

Between Phase 1 and Phase 4, the UAV also requires energy for various manoeuvres, such as hovering, acceleration, deceleration and flying at a speed of V. An analytical propulsion power consumption model for rotary-wing UAVs flying at a speed of V was reported in [47] as

$$P(V) = P_0 \left(1 + \tfrac{3V^2}{U_{tip}^2}\right) + P_i \left(\sqrt{1 + \tfrac{V^4}{4v_0^4}} - \tfrac{V^2}{2v_0^2}\right)^{1/2} + \frac{d_0 \rho s A V^3}{2}, \tag{15}$$

where P_0 and P_i are two constants related to the physical properties of UAV and the flight environment, such as weight, rotor radius and air density, Other parameters are detailed in [47]. Denote the energy consumption during acceleration, deceleration and flying as E_{Acc}, E_{Dec} and E_V, respectively. By substituting $V = 0$ into (15), the power consumption for hovering can be obtained as $P(0) = P_0 + P_i$. Thus, E_{hover} and E_V can be calculated by multiplying power by time. In this study, we consider the process when the UAV accelerates from an initial velocity of 0 to V and continues to fly to the sensors at the speed of V, and finally decelerates from V to 0 to hover over the sensors. Hence, the energy consumed by the UAV during the acceleration can be calculated approximately as [32] and [48] as

$$E_{Acc} = \int_0^{\frac{V}{a}} P\left[V(t)\right] \, dt, \tag{16}$$

where a is acceleration. Since acceleration and deceleration in this study are symmetric, the energy consumed during deceleration is the same as that during acceleration, i.e., $E_{Acc} = E_{Dec}$. Note that (16) is valid only for forward level flight as specified in [47]. For vertical flight and arbitrary 2D level flight, the energy consumption can be calculated using [48, eq. (3)] and [49, eq. (12)], respectively. As a result, complex path planning for the UAV may consume more energy and thus, affects the system performance. This will be considered as future work.

F. Compound Convex Optimization Problem

It is challenging to directly optimize the time allocation among the above four phases to maximize the amount offloaded to the BS, because this target is constrained by both time and energy. The convergence of the target function can not be guaranteed. However, it is found that more data collected by the UAV is a necessary condition for maximizing the data offloaded to the BS. Thus, the target can be regarded as two sub-problems and both are convex. As a result, the target optimization problem can be solved in the following two steps.

1) Step 1: We first maximize the data collected by the UAV, i.e., optimize the time allocation between Phase 2 and Phase 3 [30].

2) Step 2: Once the optimal time ratio between Phase 2 and Phase 3 is derived, it can be combined and taken as a whole. In doing so, the original optimization can be regarded as a time allocation problem with only three processes, i.e., Phase 1, "Phase 2 and Phase 3", and Phase 4.

III. Problem formulation and Optimization

In this section, we will solve an optimization problem that maximizes the amount of data offloaded at the BS to derive the closed-form expression of the optimal time allocation for the four phases described in Fig. 1. To analyse the performance of this process, two cases will be studied. In Case 1, TDMA with optimal transmission times for all sensors is studied. While in Case 2, TDMA with equal transmission times for all sensors is considered.

A. Case 1

In Phase 1, the UAV hovers above the BS to be charged. It is assumed that the initial position of the UAV is $(0, 0, H)$ with the minimum initial energy of the system E_ϵ. Since the UAV consumes power for keeping aloft (i.e., hovering) while being charged, the sum energy harvested by the UAV at the end of T_{phase1} can be calculated as

$$E_0 = E_\epsilon + E_{uav-h} - E_{hover1}, \tag{17}$$

where E_{uav-h} is the energy harvested by the UAV from the BS in (2) with $E_{uav-h} > E_{hover1}$, $E_{hover1} = P(0) \cdot T_{phase1}$ is the energy consumed by hovering in Phase 1, $P(0)$ is the power for hovering and T_{phase1} is the hovering time. We denote as E_{fly-to} and $E_{fly-back}$ the energy consumed by the UAV flying to the sensors and flying back to the BS, respectively. One has

$$E_{fly-to} = E_{fly-back} = E_{Acc} + E_V + E_{Dec}. \tag{18}$$

In Phase 2, the UAV broadcasts wireless energy to the sensors by WPT. The total energy transferred from the UAV can be calculated as

$$E_{wpt} = 10^{\frac{P_{uav-t}}{10}} * T_{phase2}, \tag{19}$$

and the energy consumed for hovering during this process is

$$E_{hover2} = P(0) * T_{phase2}. \tag{20}$$

After this, the sensors start to transmit their data to the UAV via TDMA using the harvested energy.

In Phase 3, the UAV still needs to keep aloft while receiving data from the sensors. Hence, it continues consuming energy in hovering as

$$E_{hover3} = P(0) * T_{phase3}. \tag{21}$$

Next, the UAV flies back to the BS with the collected data to consume an amount of energy $E_{fly-back}$ given in (18).

In Phase 4, when the UAV reaches the BS, the available energy at the UAV is

$$E_{available} = E_0 - E_{fly-to} - E_{fly-back} - E_{wpt} - E_{hover2} - E_{hover3}. \quad (22)$$

To deliver as much data collected from the sensors to the BS as possible, $E_{available} - E_\epsilon$ will be used for offloading. The reason to keep an amount of energy E_ϵ at the end of offloading is to prepare the UAV for the next round of data collection. Hence, $E_{available} \geq E_\epsilon$. Meanwhile, since the UAV has to keep hovering, the offloading time for Phase 4 can be calculated as

$$T_{phase4} = \frac{E_{available} - E_\epsilon}{P(0) + 10^{\frac{P_{uav-t}}{10}}}, \quad T_{phase4} \geq 0. \quad (23)$$

Based on the above discussion, we can finally formulate the time allocation problem that maximizes the amount of data received by the BS under the constraint of a fixed time $\tau = T - T_{flying}$, where T is the total time and T_{flying} is the time for round trip which is determined by the flight distance and UAV speed and both are fixed. The variables to be optimized are T_{phase1}, T_{phase2}, T_{phase3} and T_{phase4}. As a result, the problem is formulated as

$$(P1): \max_{T_{phase1}, T_{phase2}, T_{phase3}, T_{phase4}} D_{u,b}, \quad (24a)$$

$$\text{s.t.: } 0 \leq T_{phase1} \leq \tau, \quad (24b)$$

$$0 \leq T_{phase2} \leq \tau, \quad (24c)$$

$$0 \leq T_{phase3} \leq \tau, \quad (24d)$$

$$0 \leq T_{phase4} \leq \tau, \quad (24e)$$

$$E_{available} \geq E_\epsilon, \quad (24f)$$

$$D_{u,b} \leq D_{K,u}, \quad (24g)$$

$$\tau = T_{phase1} + T_{phase2} + T_{phase3} + T_{phase4}, \quad (24h)$$

where (24a) is the objective function, (24b) – (24e) are the constraints on T_{phase1}, T_{phase2}, T_{phase3} and T_{phase4}, (24f) is the constraint on available energy at the UAV in Phase 4 given by (17) and it has already included the constraint $E_{uav-h} > P(0) \cdot T_{phase1}$ in (17), (24g) is the constraint on data volume between $D_{u,b}$ and $D_{K,u}$ that the amount of received data cannot exceed the amount of collected data, and (24h) is the constraint on the fixed time τ.

The optimization problem in (24) is complicated because the objective function is constrained by both energy and time and its convergence cannot be guaranteed. This can be explained as follows. With given T_{phase1}, T_{phase2} and T_{phase3}, T_{phase4} can be derived by (24h). However, T_{phase4} is also given by (23), the one for offloading data in Phase 4 with energy constraint included in (24f). It does not necessarily imply that the two are equal. When the one from (24h) is greater than the one from (23), it means there is a waste of time as the energy determines the time that can be used to offload data. Besides, it may be noted that $D_{K,u}$ is actually determined by T_{phase2} and T_{phase3} as T_{phase2} determines the energy used to transmit data from sensors to the UAV in Phase 3. Thus, the time allocation between T_{phase2} and T_{phase3} should be carefully chosen. Once this optimal allocation is derived, then they can be considered as a whole for optimizing the allocation of τ. To this end, we decompose this optimization into two steps.

B. Solution to the Case 1

1) Step 1: In order to maximize the amount of data received at the BS, we first optimize the time allocation between T_{phase2} and T_{phase3} to maximize the amount of data received from sensors by fixing $T_{phase2} + T_{phase3}$. To do this, denote $T_{phase2\&3} = T_{phase2} + T_{phase3}$ as the sum of T_{phase2} and T_{phase3}, and $\mu_2 = \frac{T_{phase2}}{T_{phase2\&3}}$ and $\mu_3 = \frac{T_{phase3}}{T_{phase2\&3}}$ as the proportions of T_{phase2} and T_{phase3} in the sum, respectively. Once the optimal values of μ_2 and μ_3 are derived as μ_2^* and μ_3^*, the optimal time allocation of T_{phase2} and T_{pahse3} can be obtained as $\mu_2^* * T_{phase2\&3}$ and $\mu_3^* * T_{phase2\&3}$, respectively, for fixed $T_{phase2\&3}$ in this step. Mathematically, this problem after normalization of $T_{phase2\&3}$ can be formulated as

$$(P1_{-S1}): (\mu_2^*, \mu_3^*) = \arg\max_{\mu_2, \mu_3} \ \bar{D}_{K,u}(\mu_2, \mu_3) \quad (25a)$$

$$\text{s.t.: } \mu_2 + \mu_3 = 1, \quad (25b)$$

$$0 < \mu_2, \mu_3 < 1, \quad (25c)$$

where $\bar{D}_{K,u} = \frac{D_{K,u}}{T_{phase2\&3}}$ is the normalized maximum amount of data with respect to time. The optimization problem in (25) is different from that in [3] and [30] as they used fixed energy conversion efficiency. In our work, we assumed that the energy conversion efficiency is non-linear and depends on the input power as in (6), since the received power at each sensor is various. The transmit power of each sensor, P_{k-t}, is determined by its harvested energy from the UAV, as in [3] – [4] and [30]. To solve $(P1_{-S1})$ above, using (3) to (11) and replacing t_k in (11) with its time proportion λ_k, $(P1_{-S1})$ can be reformulated as

$$(P1_{-S1}): (\mu_2^*, \mu_3^*) = \arg\max_{\mu_2, \mu_3} \sum_{k=1}^{K} \lambda_k \log_2\left(1 + \gamma_k \frac{\lambda_0}{\lambda_k}\right) \quad (26a)$$

$$\text{s.t.: } \sum_{k=0}^{K} \lambda_k = 1, \quad (26b)$$

$$\lambda_k \geq 0, \ k = 0, \cdots, K, \quad (26c)$$

$$\mu_2 = \lambda_0, \quad (26d)$$

$$\mu_3 = \sum_{k=1}^{K} \lambda_k, \quad (26e)$$

where $\gamma_k = \frac{\eta_k 10^{\frac{P_{uav-t} + 2G_k + 2G_{uav} - 2PL_{uav-k}}{10}} |h_{u,k}|^2 |g_{k,u}|^2}{\sigma^2_{k,u}}$, $\mu_2 = \lambda_0$ is allocated to the DL WPT in Phase 2, $\lambda_k \geq 0$, $k = 1, \cdots, K$, is the time portion assigned to the k^{th} sensor and $\mu_3 = \sum_{k=1}^{K} \lambda_k$ is the total time portion for UL WIT in Phase 3. Note that, for an arbitrary topology of sensors, one needs to study the optimal location of the UAV [32], as the geometric centre may not be the middle of the area. This study is beyond the scope of the current work. Also, we do not consider UAV trajectory optimization, as in [11] and [13], because these works have ignored the UAV power consumption and the flying-to and flying-back processes while our work takes all of these into account. When UAV power consumption is considered, flying to each sensor may be disadvantageous to staying at a fixed location, due to the extra propulsion energy. Thus, the UAV will hover at one spot over the sensors.

From [30], (26) is a convex optimization problem and the optimal time allocation solution for $(P1_{-S1})$ in each block time

of $T_{phase2\&3}$, denoted by ${\lambda_k}^\star,\ k=0,\cdots,K$, is given by

$$\lambda_k{}^\star = \begin{cases} \dfrac{z^\star - 1}{\Upsilon + z^\star - 1}, & k=0, \\ \dfrac{\gamma_k}{\Upsilon + z^\star - 1}, & k=1,\cdots,K, \end{cases} \tag{27}$$

where $\Upsilon = \sum_{k=1}^{K}\gamma_k > 0$ and $z^\star$ is the solution of $z\ln z - z + 1 = \Upsilon,\ z \geq 0$ given in [30]. Hence, the values for Phase 2 and Phase 3 can be obtained as

$$\begin{cases} \mu_2^* = {\lambda_0}^\star, \\ \mu_3^* = \sum_{k=1}^{K} {\lambda_k}^\star, \end{cases} \tag{28}$$

and the optimal time allocation between Phase 2 and Phase 3 can be derived as

$$\begin{cases} T_{phase2}^* = \mu_2^* * T_{phase2\&3}, \\ T_{phase3}^* = \mu_3^* * T_{phase2\&3}. \end{cases} \tag{29}$$

Also, the maximum data volume per unit time can be obtained by substituting (27) into (26) as

$$\bar{D}_{K,u} = \sum_{k=1}^{K} {\lambda_k}^\star \log_2\left(1 + \gamma_k \frac{{\lambda_0}^\star}{{\lambda_k}^\star}\right). \tag{30}$$

2) Step 2: Once the achievable data in the sensor network is maximized in $Step\ 1$, the whole process can be treated as three phases because T_{phase2} and T_{phase3} can be combined as one phase denoted by $T_{phase2\&3} = T_{phase2} + T_{phase3}$, as $Step\ 1$. In this case, we let α and β be the ratio of T_{phase1} and $T_{phase2\&3}$ to the time $\tau = T_{phase1} + T_{phase2} + T_{phase3} + T_{phase4}$, and $(1-\alpha-\beta)$ be the ratio of T_{phase4} to τ. Thus, $\alpha = \dfrac{T_{phase1}}{\tau}$, $\beta = \dfrac{T_{phase2\&3}}{\tau}$, $1-\alpha-\beta = \dfrac{T_{phase4}}{\tau}$. As a result, the optimization problem in (24) can be rewritten as

$$\begin{aligned} (P1_{-S2}): (\alpha^*, \beta^*) = \arg\max_{\alpha,\beta}\ & D_{u,b}\ (\alpha, \beta) && \text{(31a)} \\ \text{s.t.: } & 0 \leq \alpha \leq 1, && \text{(31b)} \\ & 0 \leq \beta \leq 1, && \text{(31c)} \\ & 0 \leq \alpha + \beta \leq 1, && \text{(31d)} \\ & E_{available} \geq E_\epsilon, && \text{(31e)} \\ & D_{u,b} \leq D_{K,u}. && \text{(31f)} \end{aligned}$$

where (31a) is the objective function, (31b) – (31d) are the constraints on T_{phase1}, $T_{phase2\&3}$ and T_{phase4}, respectively, (31e) is the constraint on energy when the UAV arrives at the top of the BS in Phase 4, and (31f) is the constraint on the data volume between $D_{u,b}$ and $D_{K,u}$.

Details on the solution to $(P1_{-S2})$ is summarized in Algorithm 1. In the Algorithm, some special cases causing $D_{u,b} = 0$ has also been considered. This comes from the lack of time ($1-\alpha-\beta \leq 0$) or energy ($E_{available} \leq E_\epsilon$), or the time proportion (β) for Phase 3 is 0. Once α^* and β^* are derived from the Algorithm 1, the optimal time allocation between T_{phase1}, $T_{phase2\&3}$ and T_{phase4} can be derived as

$$\begin{cases} T_{phase1}^* = \alpha^*\tau, \\ T_{phase2\&3}^* = \beta^*\tau, \\ T_{phase4}^* = (1-\alpha^*-\beta^*)\,\tau. \end{cases} \tag{32}$$

Since the optimal time allocation proportions of T_{phase2} and T_{phase3} have been derived in $P1_{-S1}$, as μ_2^* and μ_3^*, the final optimal time allocation for the original problem $(P1)$ can be obtained as

$$\begin{cases} T_{phase1}^* = \alpha^*\tau, \\ T_{phase2}^* = \mu_2^*\beta^*\tau, \\ T_{phase3}^* = \mu_3^*\beta^*\tau, \\ T_{phase4}^* = (1-\alpha^*-\beta^*)\,\tau. \end{cases} \tag{33}$$

Algorithm 1: Optimization of (31)

Input: $\alpha = 0$: *step_*α: 1, $\beta = 0$: *step_*β: 1
Output: $D_{u,b_{max}}$, $\alpha^*(i), \beta^*(j)$

```
for i=1: length(α) do
    for j=1: length(β) do
        /* E_4 is the available energy at Phase 4
           calculated by α(i) and β(j)                    */
        if α(j) == 0 || β(j) == 0 || α(i) + β(j) ≥ 1
         then
            D_{u,b}(i,j) = 0 // Data from the UAV to
               the BS
        else
            E_4(i,j) ← calculate the rest of energy
             using α(i), β(j)
            if E_4 ≤ 0 then
                D_{u,b}(i,j) = 0
            /* Compare the actual remaining time
               with the original planned
               allocation time                            */
            else if
             E_4(i,j)/(P_{uav-t}+P_hover) ≥ (1 − α(i,j) − β(i,j)) τ
             then
                /* TP_ub is the throughput from the
                   UAV to the BS                          */
                if (1 − α(i,j) − β(i,j))τ * TP_ub ≥
                 β(j)τ * D̄_{K,u} then
                    D_{u,b}(i,j) = β(j)τ * D̄_{K,u}
                else
                    D_{u,b}(i,j) =
                     (1 − α(i,j) − β(i,j))τ * TP_ub
            else
                if E_4(i,j)/(P_{uav-t}+P_hover) * TP_ub ≥ β(j)τ * D̄_{K,u}
                 then
                    D_{u,b}(i,j) = β(j)τ * D̄_{K,u}
                else
                    D_{u,b}(i,j) = E_4(i,j)/(P_{uav-t}+P_hover) * TP_ub
```

Result: $D_{u,b_{max}} = \max D_{u,b}(i,j), \alpha^*(i), \beta^*(j) \leftarrow (i,j) = \arg\max D_{u,b}(i,j)$

Complexity Analysis of Algorithm 1: For Algorithm 1, the complexity to compute $D_{u,b}(i,j)$ mainly comes from the two "for" loops for parameters α and β, which are determined by the step-sizes of α or β. Assume that the number of iterations of the first "for" loop is m, and the second "for" loop is n.

The complexity of Algorithm 1 is

$$\boldsymbol{O}\left(m \times n\right), \tag{34}$$

where $m = \frac{1}{step\_\alpha} + 1$, $n = \frac{1}{step\_\beta} + 1$.

C. Case 2

Compared with Case 1, in this case, the time allocated to each sensor is the same in Phase 3. Hence, there is no optimal time allocation for each sensor in Phase 3. This simplifies the network synchronization. As discussed in [30], there is always a "near-far" issue that affects the fairness among users. In [30], this was tackled by imposing a minimum rate on each user.

Now that the time allocated for each sensor in Phase 3 is the same, one has calculated as

$$t_k = \frac{T_{phase3}}{K}. \tag{35}$$

Consequently, the transmission power by the k^{th} sensor, denoted by P_{k-t} as in (8) can be calculated by substituting (35) into (8) as

$$P_{k-t} = \frac{E_k}{t_k} = \frac{\eta_k 10^{\frac{P_{k-r}}{10}} |h_{u,k}|^2 T_{phase2} K}{T_{phase3}}. \tag{36}$$

As other processes and the final optimization problem, i.e., maximizing $\bar{D}_{K,u}$, are the same as in Case 1, the problem is also solved in two steps.

D. Solution to the Case 2

1) Step 1: $Step$ 1 can be formulated by using $\bar{D}_{K,u} = \sum_{k=1}^{K} \frac{\mu_3}{K} \log_2\left(1 - KA_k + \frac{KA_k}{\mu_3}\right)$ and $\mu_2 = 1 - \mu_3$ as

$$\mu_3^* = \arg\max_{\mu_3} \sum_{k=1}^{K} \frac{\mu_3}{K} \log_2\left(1 - KA_k + \frac{KA_k}{\mu_3}\right), \tag{37a}$$

$$\text{s.t.: } 0 < \mu_3 < 1, \tag{37b}$$

where $A_k = \frac{\eta_k 10^{\frac{P_{uav-t} + 2G_k + 2G_{uav} - 2PL_{uav-k}}{10}} |h_{u,k}|^2 |g_{k,u}|^2}{\sigma^2_{k,u}}$. From (37), the objective function is a function of μ_3 for a given number of sensors K. This is because η_k and PL_{uav-k} in A_k can be regarded as constants given the topology of sensors. Besides, as in [30], it is assumed that both DL and UL channels are quasi-static flat-fading. Thus, $|h_{u,k}|^2$ and $|g_{k,u}|^2$ remain constant during each block in Phase 3. Note that A_k $(k = 1 \ldots K)$ are different for different sensors. Hence, $\bar{D}_{K,u}$ can be seen as a function of only one variable μ_3.

From (37), $\bar{D}_{K,u} = \sum_{k=1}^{K} \frac{\mu_3}{K} \log_2\left(1 - KA_k + \frac{KA_k}{\mu_3}\right)$ is a concave function of μ_3 and thus, this is a convex optimization problem. However, the first order derivative of (37) includes an item in the form of "$x \ln x$", and it is challenging to derive its closed-form solution when K is large. Hence, for K sensors with a given topology, one-dimensional exhaustive search will be used to derive μ_3^* and corresponding $\bar{D}_{K,u}$. This is described in Algorithm 2. For the special case of only one sensor, i.e., $K = 1$, the optimal time proportion, μ_3^*, is also derived in Appendix VI.

Complexity Analysis of Algorithm 2: For Algorithm 2, the complexity to calculate μ_3^* and $\bar{D}_{K,u}$ mainly comes from three "for" loops with indexes i, j and k. The increment index i is determined by the step-size $step\_\mu_3$, and k depends on the number of sensors K. Note that the last value of the index j is fixed, assumed to be 1000 as an example. As a result, denoting $l = \frac{1}{step\_\mu_3}$ as the number of iterations of the first "for" loop, the complexity of Algorithm 2 can be calculated as

$$\boldsymbol{O}\left(l \times 1000 \times K\right). \tag{38}$$

As a result, the optimal time proportion of T_{phase2} can then be calculated as $\mu_2^* = 1 - \mu_3^*$. Finally, the optimal time allocation for T_{phase2} and T_{phase3} can be obtained as (29).

2) Step 2: As other processes are the same as those in Case 1, the optimal time allocation for Phases 1 to 4 can be derived following the steps in Step 2 of Case 1.

Algorithm 2: Optimization of (37)

Input: μ_3 =Initial value: $step\_\mu_3$: $1, G_k, G_{uav}, r, R, K, P_{uav-t}, \sigma^2_{k,u}$, Sum_$\bar{D}_{K,u}$, Average_$\bar{D}_{K,u}$, temp_$\bar{D}_{K,u}$, $\bar{D}_{K,u}$=0

Output: μ_3^*, $\bar{D}_{K,u}$

for *i=1*: *length*(μ_3) **do**
  Initialize Sum_$\bar{D}_{K,u} = 0$
  for *j=1:1000* **do**
    for *k=1:K* **do**
      // PDF_{Rician} is Probability Density Function of Rician distribution
      $h_{u,k}(k) = random(PDF_{Rician}, 1, 1)$
      $g_{k,u}(k) = random(PDF_{Rician}, 1, 1)$
      Calculate A_k
    Calculate temp_$\bar{D}_{K,u}(j)$=$\sum_{k=1}^{K} \bar{D}_{k,u} \leftarrow$ using $\mu_3(i)$
    Sum_$\bar{D}_{K,u}$ = Sum_$\bar{D}_{K,u}$ + temp_$\bar{D}_{K,u}(j)$
  Average_$\bar{D}_{K,u}(i)$ = $\frac{Sum\_\bar{D}_{K,u}}{1000}$
  if $\bar{D}_{K,u} < Average\_\bar{D}_{K,u}(i)$ **then**
    $\bar{D}_{K,u}$ = Average_$\bar{D}_{K,u}(i)$
    $\mu_3^* = \mu_3(i)$

Result: μ_3^*, $\bar{D}_{K,u}$

IV. Further Discussion

A. Wired Charging

Case 1 and Case 2 are the cases when there is no dedicated landing dock at the BS for wired charging or when it is not convenient or safe for the UAV to land due to the complicated environment. They require wireless charging. In this subsection, we discuss the case when wired charging is available.

1) Case 3: Following the discussion in Case 1, the UAV is first charged by the BS via a wired connection and thus, T_{phase1} will be greatly reduced because of high energy conversion efficiency. However, there may be an extra vertical flight when the height of the BS is lower than H, which in turn increases T_{flying} and consumes extra energy. Upon arrival, the method in $Step1$ of Case 1 is still valid and can be used to derive the optimal time proportion, μ_2^* and μ_3^*, for the WPT phase and the WIT phase. In this case, T_{phase4} can be ignored because of the wired connection. As a result, $\tau = T - T_{flying} = T_{phase1} + T_{phase2\&3}$. To maximize the data offloaded to the BS, one needs to balance the relationship between time and energy. Specifically, with small

T_{phase1}, E_0 is also small. In this regime, as E_0 increases with increasing T_{phase1} until it is fully charged. However, as T_{phase1} increases, $T_{phase2\&3}$ is decreased. As a result, the amount of data collected from sensors will be limited by time. In turn, it will be limited by energy. Therefore, there exists an optimal time allocation between T_{phase1} and $T_{phase2\&3}$. One has the following relationship

$$\begin{cases} \tau = T_{phase1} + T_{phase2\&3}, \\ E_{available} = E_\epsilon. \end{cases} \tag{39}$$

2) Case 4: In this case, we not only use wired charging to replace wireless charging as in Case 3, but also allocate equal times to the K sensors, as in Case 2. Thus, the optimal values of μ_2^* and μ_3^* in this are derived by Algorithm 2, instead of from equations (27) and (28). As other processes and steps are the same as those in the previous subsection, they will not be discussed further. It can be noted that, for the case of wired charging, T_{phase4} can be ignored as the collected data can be transmitted to the BS by a wired connection. Thus, more time can be used for WPT and WIT in Phases 2 and 3, respectively.

B. Transmission Efficiency

Using (11) and (14), the transmission efficiency of the UAV-aided data collection system can be defined as

$$TE = \frac{D_{u,b}}{D_{K,u}} = \frac{T_{phase4}\log_2\left(1+\frac{10^{\frac{P_{bs-r}}{10}}|h_{u,b}|^2}{\sigma_{u,b}^2}\right)}{\sum_{k=1}^{K} t_k \log_2\left(1+\frac{10^{\frac{P_{uav-r_k}}{10}}|g_{k,u}|^2}{\sigma_{k,u}^2}\right)}. \tag{40}$$

In Section III, we have first maximized $D_{K,u}$ in (25) and then maximized $D_{u,b}$ in (31). The value of $D_{u,b}$ is always smaller than or equal to $D_{K,u}$. Thus, $TE \leq 1$. When $TE < 1$, there is some data loss, as the amount of data offloaded to the BS is smaller than the data collected from the sensors. Ideally, all the collected data should be delivered to the BS so that the transmission efficiency should be 1. Transmission efficiency of 1 does not guarantee that the data received by the BS is the maximum and vice versa. This is because there are many ways of achieving a transmission efficiency of 1. For example, the UAV can choose to collect a minimum amount of data from the sensors to be fully delivered to the BS so that both $D_{u,b}$ and $D_{K,u}$ are small but no data is lost for reliability to achieve a transmission efficiency of 1. Therefore, we can let the transmission efficiency be 1, and let time for Phase 4 all be used to offload the data. One has

$$\begin{cases} D_{u,b} = D_{K,u}, \\ E_{available} - E_\epsilon = (1-\alpha-\beta)\tau * \left(P(0) + 10^{\frac{P_{uav-t}}{10}}\right). \end{cases} \tag{41}$$

Therefore, the optimal allocation can be derived by solving (41) as

$$\begin{aligned} \alpha^* &= \frac{MF - NW}{MF - NE}, \\ \beta^* &= \frac{MW - ME}{MF - NE}, \end{aligned} \tag{42}$$

Table I: Simulation Parameters

Notation	Parameters	Values
α	The ratio of T_{phase1} to the τ	—
β	The ratio of $T_{phase2\&3}$ to the τ	—
K	Rician factor	10 dB
P_{bs-t}	Transmit power at the BS	35.68 dBW
P_{uav-t}	Transmit power at the UAV	40 dBm
G_{bs}	Antenna gain of the BS	15 dBi
G_{uav}	Antenna gain of the UAV	5 dBi
G_k	Antenna gain of the k^{th} sensor	5 dBi
H_{bs}	The height of the BS	4.5 m
H_{sr}	Sensors antenna height	0.5 m
H	Flight height of the UAV	5.5 m
f	Operating frequency	915 MHZ
v	UAV speed	10 m/s
a	Acceleration/deceleration	1 m/s^2
a_0	Model parameter in (5)	2.463
b_0	Model parameter in (5)	1.635
c_0	Model parameter in (5)	0.826
$\sigma_{b,u}, \sigma_{u,b}$	Noise power	-80 dBm
$\sigma_{u,k}, \sigma_{k,u}$	Noise power	-80 dBm

where $M = \log_2\left(1+\frac{10^{\frac{P_{bs-r}}{10}}|h_{u,b}|^2}{\sigma_{u,b}^2}\right)$, $N = M + \bar{D}_{K,u}$, $W = E_{fly-to} + E_{fly-back} + P(0)\tau + 10^{\frac{P_{uav-t}}{10}}\tau$, $E = \eta 10^{\frac{P_{uav-r}}{10}}|g_{b,u}|^2\tau + 10^{\frac{P_{uav-t}}{10}}\tau$, $F = \mu_3^*\tau 10^{\frac{P_{uav-t}}{10}}$. This solution ensures that all data collected from sensors will be offloaded to the BS without wasting any time and energy. For Cases 1 and 2 in wireless charging, the solution in (42) depends on μ_2^* and μ_3^* derived from (28) or Algorithm 2 although it has closed-form. Moreover, the random complex channel coefficient $h_{u,k}$ and $g_{k,u}$ also determines the solution in (42). Thus, it is dependent.

V. Numerical Results and Discussion

In this section, numerical results are presented to show the optimal time allocation maximizing the amount of data received by the BS. The simulation settings are similar to [31], [32], [47] and [50], and the detailed settings are summarized in Table I. The average rate is obtained by generating 1000 random values of $|h_{u,k}|^2|g_{k,u}|^2$, adding them together and dividing the sum by 1000. For $|h_{b,u}|^2$ or $|g_{u,b}|^2$, the average value of 1000 random values is also taken. The total operating time τ including all phases and round trip flight is set to 3600 s. The RF-to-DC conversion efficiency from the BS to the UAV $\eta \approx 0.8$. The flight distance is set to 1000 m and the parameters of the UAV follow [32, Table I].

Fig. 3 shows the effects of α and β on the data volume at the BS. In this figure, we take one sensor as an example. The upper part of the figure shows the data volume at the BS versus α, which is the charging time proportion in Phase 1, when β is fixed. One can see that all the curves look like a "square wave", as expected. This can be explained as follows. When α is small, the amount of energy harvested by the UAV from the BS is small, which will lead to the following results: i) the UAV has too little energy to fly to the sensors; ii) the UAV has no energy to receive data from the sensors, otherwise it

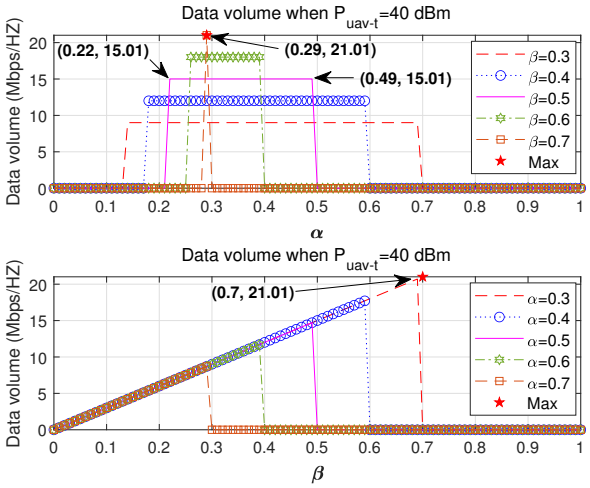

Fig. 3. The influence of α and β on data volume, respectively.

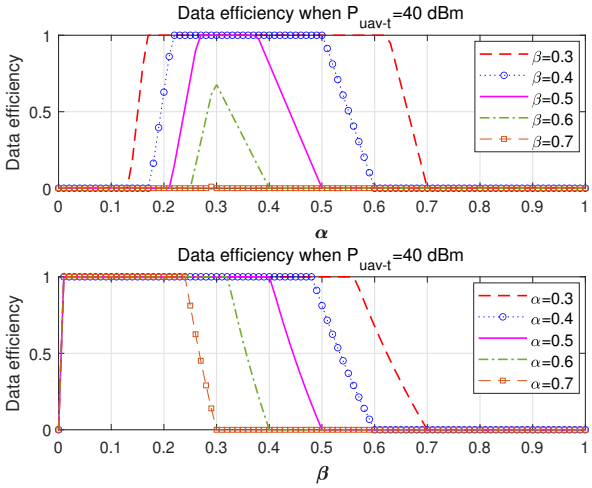

Fig. 4. The influence of α and β on transmission efficiency, respectively.

cannot fly back; iii) the UAV can only fly back, but there is no energy to offload data to the BS. Therefore, the data volume is 0. When α is large, the UAV has enough energy but there is limited time for WPT and WIT. This may lead to 1) no time to receive data from the sensors; 2) no time to fly back; 3) no time to deliver the received data to the BS. As a result, there is no data received by the BS either. When α is medium, reasonable values of α are available for fixed β. Take $\beta = 0.5$ as an example. The data volume remains unchanged when α increases from 0.22 to 0.49, which means $\alpha = 0.22$ is the minimum time portion requirement in this setting. Otherwise, there will be energy surplus after data delivery, such as when $\alpha = 0.4$. The lower part of the figure shows the data volume at the BS versus β, which is the proportion of the total time of Phase 2 and Phase 3 for WPT and WIT, when α is fixed. One sees that the data volume firstly increases with the increase of β, but then decreases to 0, because when α is fixed, the time for Phase 4, $1-\alpha-\beta$, decreases with increasing β. Take the case when $\alpha = 0.4$ as an example. The data volume increases when the value of β increases from 0 to 0.5. When $\beta = 0.6$, the data volume is 0. This is because there is no time left in Phase 4, i.e. $1-\alpha-\beta = 0$. According to the Algorithm 1, the optimal α^* and β^* in this example are 0.29 and 0.7, respectively, as shown in the figure, and the maximum of data volume is 21.01.

Fig. 4 shows the effects of α and β on the transmission efficiency. Also, one sensor is used in this figure as a case study. The upper part of the figure shows the transmission efficiency at the BS versus α when β is fixed. One sees that all the curves start from 0 when β changes from 0.3 to 0.5, and then rise from 0 to 1 and remain unchanged at 1, until it drops from 1 to 0 again. This is explained as follows. When α is small, the amount of energy harvested by the UAV is also small so that there is no energy left for WPT and WIT, or for Phase 4. Therefore, no data can be received by the BS, resulting in an efficiency of 0. For example, when $\beta = 0.7$, α is less than 0.3 and it makes efficiency of almost 0. When α is large, although the UAV has enough energy, there is no time left for Phase 4, as $1-\alpha-\beta$ decreases with increasing α when β is fixed. Besides, when β increases from 0.3 to 0.5, one sees that the range for α in which the transmission efficiency remains at one narrows. In particular, when $\beta = 0.6$, the transmission efficiency is less

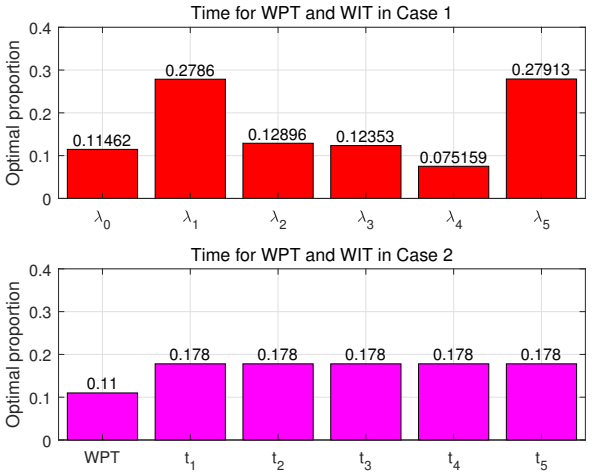

Fig. 5. The optimal time proportion of WPT and WIT, Case 1 versus Case 2.

than 1. This can also be explained from $1-\alpha-\beta$. The lower part of the figure shows the transmission efficiency versus β when α is set from 0.3 to 0.7. Similar observations can be made.

Note that, although the transmission efficiency is 1, it does not mean that the data volume is maximized. On the other hand, a large data volume does not mean that the transmission efficiency is 1 either. Thus, Figs. 3 and 4 provide very useful guidance on the choices of α and β to either maximize data volume or ensure transmission efficiency. For example, in monitoring applications for prediction, all sensing data are necessary. Hence, it is of great importance to ensure that all the sensing data collected by the UAV can be delivered to the BS. In data sampling applications for big data analysis, collecting as much data as possible and ensuring data diversity are two priorities but there is redundancy in data to allow loss. Therefore, it is important to choose reasonable values of α and β to meet different requirements.

Fig. 5 compares the optimal time proportion for WPT in Phase 2 and WIT in Phase 3, i.e., μ_2^* and μ_3^*, for Case 1 and

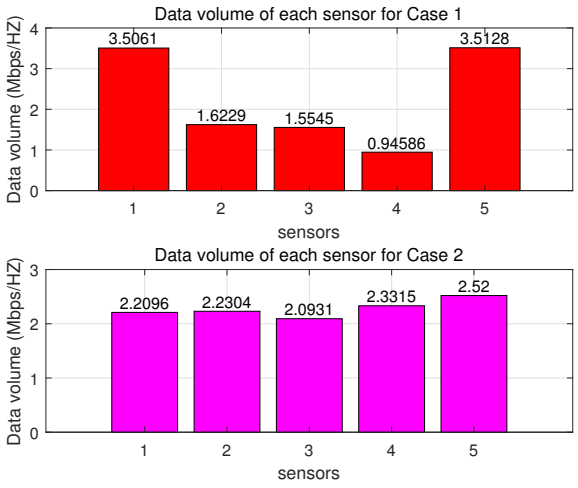

Fig. 6. Data volume of each sensor, Case 1 versus Case 2.

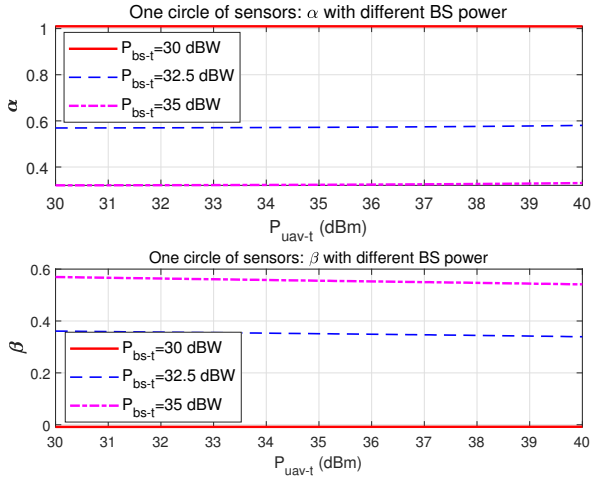

Fig. 7. The influence of P_{uav-t} on α^* and β^*.

Case 2. In the figure, we take five sensors located on a circle with a radius of 1 meter as an example. The upper part of the figure shows the optimal time proportion of WPT and WIT for each sensor, labelled as λ_0^* and λ_k^* respectively in (27) and (28). To maximize throughput, the time allocated for each sensor for WIT mainly depends on the channel state. As shown in the figure, the channel state between the UAV and the 1^{st} and 5^{th} sensors are the best among the five sensors so that their time proportion, i.e., 0.2786 and 0.27913, is the largest. On the contrary, the 4^{th} sensor has the worst channel state and thus, its time proportion is the smallest. The lower part of the figure shows the optimal time proportion in Case 2 with equal times for different sensors. As shown in the figure, the time proportion for each sensor is equal to 0.178, and the ratio of WPT to WIT is $0.11/0.89$, which is a bit small than that in Case 1.

Fig. 6 shows the data volume received from each sensor with time proportion from Fig. 5 per unit time in Case 1 and Case 2. The upper part of the figure shows the data sent by each sensor in Case 1, using the same allocation ratio as in Fig. 5. One sees that the data volume sent by each sensor is proportional to its allocated time and harvested energy. As the 5^{th} sensor is allocated the largest proportion of 0.27913 shown in Fig. 5, its transmitted data is 3.5128, which is also the largest. The lower part of the figure shows the data sent by sensors in Case 2, the same observation can be made. However, the data volume sent by each sensor varies due to different channel conditions. From the viewpoint of data volume, the total amount of data in Case 1 is very close to that in Case 2. However, there is a data imbalance in Case 1. For example, the data received from the 5^{th} sensor, i.e., 3.5128, is much greater than 0.94586 from the 4^{th} sensor. Case 2 shows a better balance in terms of data volume among all sensors, because sensors in Case 2 have the same time allocated for transmitting data. Therefore, it is of great importance to choose Case 1 or Case 2 to meet different application requirements.

Fig. 7 studies the effect of P_{uav-t} on the optimal time allocation (α^*, β^*). In the figure, we take five sensors located on a circle with a radius of 10 meters as an example, and Algorithm 2 and equation (42) are used. Unless otherwise specified, this topology is also used as an example in Fig. 8.

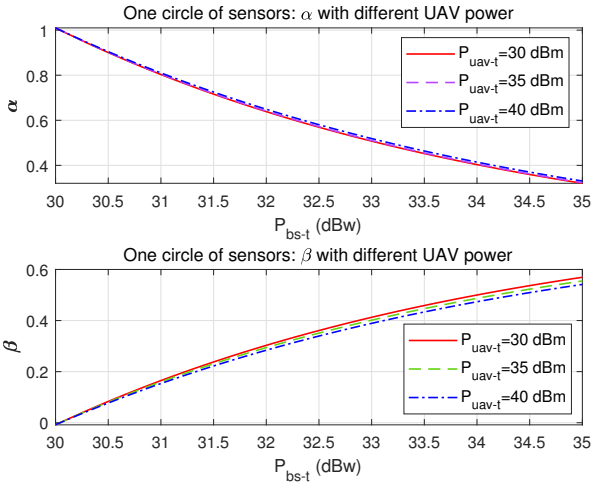

Fig. 8. The influence of P_{bs-t} on α^* and β^*.

The upper part of the figure shows the influence of P_{uav-t} on α^* when P_{bs-t} is set as 30 dBW, 32.5 dBW and 35 dBW. One sees that the optimal value of α^* increases with increasing P_{uav-t}, because larger transmitting power needs more energy reserve. When P_{uav-t} is fixed, one can see that the higher the transmitting power of the BS, the smaller the value of α^* will be. This is because the power is inversely proportional to the time when the total required energy is fixed. Note that, when $P_{bs-t} = 30dBW$, due to the path loss, it is too small to fully charge the UAV. As a result, it needs more time. This is why the solid line above 1, although it is not reasonable as $0 \leq \alpha \leq 1$. The lower part of the figure shows the influence of P_{uav-t} on β^* when P_{bs-t} is set as 30 dBW, 32.5 dBW and 35 dBW. One sees that the value of β^* decreases with increasing P_{uav-t}, because the increase of P_{uav-t} leads to increased α^*, while β^* decreases with increasing α^* when the time for Phase 4, $1 - \alpha^* - \beta^*$, is fixed. Besides, when P_{uav-t} is fixed, one can see that β^* increases with increasing P_{bs-t} as large P_{bs-t} leads to smaller α^*, thereby resulting in increased β^*. Also, the solid line shows that when $P_{bs-t} = 30$ dBW, it is not enough to fully charge the UAV as explained aforementioned.

Fig. 8 examines the effects of P_{bs-t} on α^* and β^*, respec-

tively. The upper part and the lower part of the figure show the opposite trend as those in Fig. 7. In other words, both Fig. 7 and Fig. 8 imply that the increase of P_{bs-t} will decrease α^* and increase β^*, whilst the increase of P_{uav-t} will increase α^* and decrease β^*. Note that, changes to α^* and β^* will have an impact on data volume. Thus, we next investigate the effects of P_{bs-t} and P_{uav-t} on the data volume.

VI. Conclusion

In this paper, we have studied the optimal time allocation for the UAV-aided data collection, where the BS charging process for the UAV, the UAV's propulsion consumption and the data offloading process are all taken into account. By maximizing the data volume and analysing the transmission efficiency, the optimal time allocation in different phases has been derived. When the total time is fixed, we have also derived the closed-form expression of the optimal time allocation. Numerical results have shown that the optimal α^* and β^* can maximize the data volume without wasting any time or energy. These results have provided very useful guidance for UAV-enabled WPCN system designs. As future work, it would be interesting to consider the impact of hovering fluctuation. To this end, the effect of antenna directivity gain under different UAV channel conditions needs to be considered. Besides, it is also interesting and challenging to consider the age of information in sensors with limited memory in time-limited UAV tasks.

Appendix A

Taking the first-order derivative of $\bar{D}_{K,u}$ from (37) with respect to μ_3 and let it be zero, one has

$$\frac{\partial \bar{D}_{K,u}}{\partial \mu_3} = 0 \Longleftrightarrow x_1 \ln x_1 = \frac{A_1}{\mu_3},\ x_1 = 1 - A_1 + \frac{A_1}{\mu_3}, \quad (43)$$

By observing (43), it is very challenging to derive its analytical solution. However, it is found that there is a 'function' in the form of '$x \ln x$' on the left side of the equations above, and it can be replaced by a polynomial derived by curve fitting. In this way, the approximate solution of the equation (43) can be obtained, one has

$$x_1 \ln x_1 \approx p_1 {x_1}^2 + p_2 x_1 + p_3, \quad (44)$$

where p_1, p_2 and p_3 are coefficients of the approximate polynomial. Using (44) and substitute it to (43), the optimal μ_3 can be derived as

$$\mu_3^* = \frac{-b_1 \pm \sqrt{{b_1}^2 - 4a_1c_1}}{2a_1}, \quad (45)$$

where $a_1 = p_1(1-A_1)^2 + p_2(1-A_1) + p_3$, $b_1 = 2p_1A_1(1-A_1) + p_2A_1 - A_1$, $c_1 = p_1A_1$.

References

[1] S. H. Alsamhi et al., "Green IoT using UAVs in B5G Networks: A Review of Applications and Strategies," *Ad Hoc Networks*, vol. 117, Mar. 2021.

[2] A. Khalili, E. M. Monfard, S. Zargari, M. R. Javan, N. Mokari, and E. A. Jorswieck, "Resource Management for Transmit Power Minimization in UAV-Assisted RIS HetNets Supported by Dual Connectivity," Jun. 2021, Accessed: Jun. 30, 2021. [Online]. Available: http://arxiv.org/abs/2106.13174.

[3] M. Jiang, Y. Li, Q. Zhang, and J. Qin, "Joint Position and Time Allocation Optimization of UAV Enabled Wireless Powered Communication Networks," *IEEE Trans. Commun.*, vol. 67, no. 5, pp. 3806-3816, May 2019.

[4] T. Shen and H. Ochiai, "A UAV-Aided Data Collection for Wireless Powered Sensor Network over Rician Fading Channels," in *2019 16th IEEE Annual Consumer Communications and Networking Conference, CCNC 2019*, pp. 1–5, 2019.

[5] Y. Pang, Y. Zhang, Y. Gu, M. Pan, Z. Han, and P. Li, "Efficient data collection for wireless rechargeable sensor clusters in Harsh terrains using UAVs," in *2014 IEEE Global Communications Conference, GLOBECOM 2014*, 2014, pp. 234–239.

[6] S. Arabi, H. Elbiaze, E. Sabir, and M. Sadik, "Tradeoffs for Data Collection and Wireless Energy Transfer Dilemma in IoT Environments," in *2018 IEEE International Conference on Communications (ICC)*, 2018, pp. 1–6.

[7] J. Hou, Z. Yang, and M. Shikh-Bahaei, "Energy-Efficient Data Collection and Wireless Power Transfer Using A MIMO Full-Duplex UAV," Nov. 2018. [Online]. Available: https://arxiv.org/abs/1811.10134.

[8] Y. Liu, K. Xiong, Y. Lu, Q. Ni, P. Fan, and K. Ben Letaief, "UAV-aided Wireless Power Transfer and Data Collection in Rician Fading," *IEEE J. Sel. Areas Commun.*, pp. 1–1, 2021, doi: 10.1109/JSAC.2021.3088693.

[9] Z. Wang, R. Liu, Q. Liu, J. S. Thompson, and M. Kadoch, "Energy Efficient Data Collection and Device Positioning in UAV-Assisted IoT," *IEEE Internet Things J.*, vol. 7, no. 2, pp. 1122-1139, Feb. 2020.

[10] S. Liu, Z. Wei, Z. Guo, X. Yuan and Z. Feng, "Performance Analysis of UAVs Assisted Data Collection in Wireless Sensor Network," *2018 IEEE 87th Vehicular Technology Conference (VTC Spring)*, Porto, Portugal, 2018, pp. 1-5, doi: 10.1109/VTCSpring.2018.8417673.

[11] C. You and R. Zhang, "3D Trajectory Optimization in Rician Fading for UAV-Enabled Data Harvesting," *IEEE Trans. Wireless Commun.*, vol. 18, no. 6, pp. 3192–3207, 2019.

[12] S. Goudarzi, N. Kama, M. H. Anisi, S. Zeadally, and S. Mumtaz, "Data collection using unmanned aerial vehicles for Internet of Things platforms," *Comput. Electr. Eng.*, vol. 75, pp. 1–15, May 2019.

[13] M. Samir, S. Sharafeddine, C. Assi, T. Nguyen, and A. Ghrayeb, "UAV Trajectory Planning for Data Collection from Time-Constrained IoT Devices," *IEEE Trans. Wireless Commun.*, vol. 19, no. 1, pp. 34-46, Jan. 2020.

[14] H. Q. Pham, M. Camey, K. D. Pham, K. V. Pham, and L. R. Rilett, "Review of Unmanned Aerial Vehicles (UAVs) Operation and Data Collection for Driving Behavior Analysis," *Springer, Singapore*, pp. 1111–1116, 2020.

[15] C. Zhan, Y. Zeng, and R. Zhang, "Energy-Efficient Data Collection in UAV Enabled Wireless Sensor Network," *IEEE Wireless Commun. Lett.*, vol. 7, no. 3, pp. 328–331, Jun. 2018.

[16] C. Zhan and Y. Zeng, "Completion Time Minimization for Multi-UAV-Enabled Data Collection," *IEEE Trans. Wireless Commun.*, vol. 18, no. 10, pp. 4859–4872, Oct. 2019.

[17] J. Gong, T.-H. Chang, C. Shen, and X. Chen, "Flight Time Minimization of UAV for Data Collection Over Wireless Sensor Networks," *IEEE J. Sel. Areas Commun.*, vol. 36, no. 9, pp. 1942–1954, Sep. 2018.

[18] X. Ma, R. Kacimi, and R. Dhaou, "Fairness-aware UAV-assisted data collection in mobile wireless sensor networks," in *2016 International Wireless Communications and Mobile Computing Conference (IWCMC)*, Sep. 2016, pp. 995–1001.

[19] W. Li, L. Wang, and A. Fei, "Minimizing Packet Expiration Loss with Path Planning in UAV-Assisted Data Sensing," *IEEE Wireless Commun. Lett.*, vol. 8, no. 6, pp. 1520–1523, Dec. 2019.

[20] Z. Jia, X. Qin, Z. Wang, and B. Liu, "Age-based path planning and data acquisition in UAV-Assisted IoT networks," in *2019 IEEE International Conference on Communications Workshops, ICC Workshops 2019 - Proceedings*, May 2019.

[21] J. Li, H. Zhao, H. Wang, F. Gu, J. Wei, H. Yin, B. Ren, "Joint Optimization on Trajectory, Altitude, Velocity, and Link Scheduling for Minimum Mission Time in UAV-Aided Data Collection," *IEEE Internet Things J.*, vol. 7, no. 2, pp. 1464–1475, Feb. 2020.

[22] J. Chen, F. Yan, S. Mao, F. Shen, W. Xia, Y. Wu, L. Shen, "Efficient Data Collection in Large-Scale UAV-aided Wireless Sensor Networks," in *2019 11th International Conference on Wireless Communications and Signal Processing (WCSP)*, Oct. 2019, pp. 1–5.

[23] C. Zhan and H. Lai, "Energy Minimization in Internet-of-Things System Based on Rotary-Wing UAV," *IEEE Wireless Commun. Lett.*, vol. 8, no. 5, pp. 1341-1344, Oct. 2019.

[24] H.-T. Ye, X. Kang, J. Joung, and Y.-C. Liang, "Optimization for Full-Duplex Rotary-Wing UAV-Enabled Wireless-Powered IoT Networks," *IEEE Trans. Wireless Commun.*, vol. 19, no. 7, pp. 5057-5072, July 2020.

[25] F. Wu, D. Yang, L. Xiao, and L. Cuthbert, "Energy Consumption and Completion Time Tradeoff in Rotary-Wing UAV Enabled WPCN," *IEEE Access*, vol. 7, pp. 79617–79635, 2019.

[26] "Wirelessly powered drone – GLOBAL ENERGY TRANSMISSION", Getcorp.com, 2020. [Online]. Available: http://getcorp.com/wirelessly-powered-drone/ (accessed May 17, 2021).

[27] S. Sekander, H. Tabassum, and E. Hossain, "Statistical Performance Modeling of Solar and Wind-Powered UAV Communications," *IEEE Trans. Mob. Comput.*, vol. 20, no. 8, pp. 2686–2700, Aug. 2021.
[28] A. Khalili, S. Zarandi, and M. Rasti, "Joint Resource Allocation and Offloading Decision in Mobile Edge Computing," *IEEE Commun. Lett.*, vol. 23, no. 4, pp. 684–687, Apr. 2019.
[29] S. Zarandi and H. Tabassum, "Delay Minimization in Sliced Multi-Cell Mobile Edge Computing (MEC) Systems," *IEEE Commun. Lett.*, vol. 25, no. 6, pp. 1964–1968, Jun. 2021.
[30] H. Ju and R. Zhang, "Throughput Maximization in Wireless Powered Communication Networks," *IEEE Trans. Wireless Commun.*, vol. 13, no. 1, pp. 418–428, 2014.
[31] H. Yan, Y. Chen, and S.-H. Yang, "Analysis of energy transfer efficiency in UAV-enabled wireless networks," *Phys. Commun.*, vol. 37, p. 100849, Dec. 2019.
[32] H. Yan, Y. Chen, and S.-H. Yang, "UAV-Enabled Wireless Power Transfer with Base Station Charging and UAV Power Consumption," *IEEE Trans. Veh. Technol.*,vol. 69, no. 11, pp. 12883-12896, Nov. 2020.
[33] A. Khalili, S. Zargari, Q. Wu, D. W. K. Ng, and R. Zhang, "Multi-Objective Resource Allocation for IRS-Aided SWIPT," IEEE Wireless. Commun. Lett., vol. 10, no. 6, pp. 1324–1328, Jun. 2021.
[34] K. Min Naing, A. Zakeri, and O. Iliev, "Wireless Energy transfer to long distance flying Intelligent Unmanned Aerial Vehicles (UAVs) using reactive power transfer techniques," *J. Multidiscip. Eng. Sci. Technol.*, vol. 7, no. 9, pp. 2458–9403, Sep. 2020.
[35] A. Al-Hourani, S. Kandeepan, and A. Jamalipour, "Modeling air-to-ground path loss for low altitude platforms in urban environments," in *2014 IEEE Global Communications Conference, GLOBECOM 2014*, Feb. 2014.
[36] A. Al-Hourani and K. Gomez, "Modeling Cellular-to-UAV Path-Loss for Suburban Environments," *IEEE Wireless Commun. Lett.*, vol. 7, no. 1, pp. 82–85, Feb. 2018.
[37] M. Monemi and H. Tabassum, "Performance of UAV-Assisted D2D Networks in the Finite Block-Length Regime," *IEEE Trans. Commun.*, vol. 68, no. 11, pp. 7270–7285, Nov. 2020.
[38] Y. Chen, N. Zhao, and M.-S. Alouini, "Wireless Energy Harvesting Using Signals From Multiple Fading Channels," *IEEE Trans. Commun.* , vol. 65, no. 11, pp. 5027–5039, Nov. 2017.
[39] X. Lu, P. Wang, D. Niyato, D. I. Kim, and Z. Han, "Wireless Charging Technologies: Fundamentals, Standards, and Network Applications," *IEEE Commun. Surv. Tutorials*, vol. 18, no. 2, pp. 1413–1452, 2016.
[40] P. Machura and Q. Li, "A critical review on wireless charging for electric vehicles," *Renew. Sustain. Energy Rev.*, vol. 104, pp. 209–234, Apr. 2019.
[41] M. Lu, M. Bagheri, A. P. James, and T. Phung, "Wireless Charging Techniques for UAVs: A Review, Reconceptualization, and Extension," *IEEE Access*, vol. 6, pp. 29865–29884, 2018.
[42] S. Anumula and A. Ganesan, "Wireless power charging of drone using vision-based navigation," *J. Navig.*, vol. 74, no. 4, pp. 838–852, Jul. 2021.
[43] Y. Yan, W. Shi, and X. Zhang, "Design of UAV wireless power transmission system based on coupling coil structure optimization," *EURASIP J. Wirel. Commun. Netw.* 2020 20201, vol. 2020, no. 1, pp. 1–13, Mar. 2020.
[44] Y. Rathod and L. Hughes, "Simulating the charging of electric vehicles by laser," *Procedia Comput. Sci.*, vol. 155, pp. 527–534, Jan. 2019.
[45] Q. Zhang, W. Fang, Q. Liu, J. Wu, P. Xia, and L. Yang, "Distributed Laser Charging: A Wireless Power Transfer Approach," *IEEE Internet Things J.*, vol. 5, no. 5, pp. 3853–3864, Oct. 2018.
[46] "Global Drone Regulations Database." https://droneregulations.info/index.html (accessed Sep. 15, 2021).
[47] Y. Zeng, J. Xu, and R. Zhang, "Energy Minimization for Wireless Communication With Rotary-Wing UAV," *IEEE Trans. Wireless Commun.*, vol. 18, no. 4, pp. 2329–2345, Apr. 2019.
[48] H. Yan, S. -H. Yang, Y. Chen and S. A. Fahmy, "Optimum Battery Weight for Maximizing Available Energy in UAV-Enabled Wireless Communications," in *IEEE Wireless Commun. Lett.*, vol. 10, no. 7, pp. 1410-1413, July 2021.
[49] H. Yan, Y. Chen, and S.-H. Yang, "New Energy Consumption Model for Rotary-Wing UAV Propulsion," *IEEE Wireless. Commun. Lett.*, vol. 10, no. 9, pp. 2009–2012, Sep. 2021.
[50] O. Arnold, F. Richter, G. Fettweis, and O. Blume, "Power Consumption Modeling of Different Base Station Types in Heterogeneous Cellular Networks," in *Future Network and Mobile Summit*, pp. 1–8, 2010.

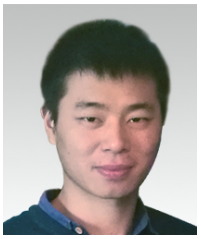

Hua Yan (S'18-M'21) received the B.E. degree in computer science from Bengbu University, Bengbu, P.R. China, and the M.S. degree in advanced computer science from Loughborough University, Loughborough, UK, in 2014 and 2017, respectively. He is currently pursuing the Ph.D. degree at the University of Warwick, U.K. His research interests include UAV-enabled wireless communications, Artificial Intelligence & Internet of Things (AIoT) and data science.

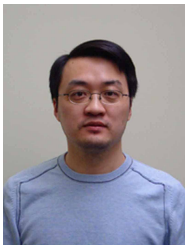

Yunfei Chen (S'02-M'06-SM'10) received his B.E. and M.E. degrees in electronics engineering from Shanghai Jiaotong University, Shanghai, P.R. China, in 1998 and 2001, respectively. He received his Ph.D. degree from the University of Alberta in 2006. He is currently working as an Associate Professor at the University of Warwick, U.K. His research interests include wireless communications, cognitive radios, wireless relaying and energy harvesting.

Shuang-Hua Yang received the B.S. degree in instrument and automation and the M.S. degree in process control from the China University of Petroleum (Huadong), Beijing, China, in 1983 and 1986, respectively, and the Ph.D. degree in intelligent systems from Zhejiang University, Hangzhou, China, in 1991. He was awarded DSc from Loughborough University in 2014 to recognize his academic contribution to wireless monitoring research. He is currently a chair professor of computer science and vice dean of graduate school with Southern University of Science and Technology (SUSTech), Shenzhen, China. Before joined SUSTech in 2016 he had spent over two decades in Loughborough University, as a professor in computer science and head of department. His current research interests include cyber-physical system safety and security, Internet of Things, wireless network-based monitoring and control. He is a Fellow of IET and a Fellow of InstMC, U.K. He is an Associate Editor of the IET Journal Cyber-Physical Systems Theory and applications, the InstMC Journal Measurement and Control, and the International Journal of Computing and Automation.